International Journal of Minerals, Metallurgy and Materials
Volume 20, Number 1, January 2013, Page 57
DOI: 10.1007/s12613-013-0693-8

Microstructure and mechanical properties of Ni-based composite coatings reinforced by in situ synthesized TiB_2 + TiC by laser cladding

Jun Li, Xuan-jun Zhang, Hui-ping Wang, and Man-ping Li

School of Materials Engineering, Shanghai University of Engineering Science, Shanghai 201620, China
(Received: 16 February 2012; revised: 18 March 2012; accepted: 12 April 2012)

Abstract: A Ni-based composite coating reinforced by in situ synthesized TiB_2 and TiC particles was fabricated on Ti6Al4V by laser cladding. An attempt was made to correlate the thermodynamic predictions and experimental observation. The microstructure and the microhardness profile across the coating were investigated by means of X-ray diffraction (XRD), scanning electron microscopy (SEM), energy dispersive spectroscopy (EDS), and a hardness tester. It is found that the coating mainly consists of a large number of reinforcements (black blocky TiB_2, flower-like or equiaxial TiC, and fine acicular CrB) and the γ matrix. The hardness of TiB_2, TiC, and CrB reinforcements is much higher than that of the γ matrix. The dispersive distribution of such high hardness reinforcements causes the increase in hardness of the whole coating. The average value of the hardness is approximately $Hv_{0.2}$ 700 in the coating. The hardness of the coating is obviously higher than that of the substrate due to the dispersion strengthening of reinforcements.

Keywords: composite coatings; laser cladding; in situ processing; microstructure; mechanical properties

1. Introduction

Titanium alloys have been widely used in aerospace, national defense, automobiles, medical care, and many other fields due to their superior strength-to-weight ratio, low density, high specific modulus, and excellent corrosion resistance [1]. However, low wear resistance and other disadvantages restrict their applications in replacing friction components under severe wear and friction conditions completely [2-3]. In recent years, in order to strengthen the engineering application of titanium alloys, the laser cladding of ceramic-metal composite coatings onto Ti-alloy substrates has been used to improve their surface properties. Cracks may propagate from the interface between ceramic particles and the metal matrix because the surface of these particles is not clean or is contaminated, so the in situ synthesis method has been extensively used to produce reinforcements on the metal matrix [4-11]. TiB_2 has high melting point, high elasticity modulus, high hardness, high temperature stability, good compatibility with metals, etc., which can make the coating have high hardness and low friction coefficient when it is used as the reinforcement for NiCrBSi alloys [12]. Compared with TiB_2, TiC can offer the necessary toughness to the coating to operate under higher loads and to remain stable at high temperature. On the other hand, TiC has a lower density, a better wettability, and a higher hardness and wear resistance [13]. There are few reports about the preparation of nickel matrix composite coatings reinforced by in situ synthesized TiB_2 and TiC on titanium alloys by laser cladding at present [14-16].

This research aims to prepare a nickel matrix composite coating reinforced by in situ synthesized TiB_2 and TiC on a Ti6Al4V substrate by laser cladding. The microstructure and microhardness profile were investigated in detail by modern analysis methods.

2. Experimental

Ti6Al4V alloy was used as the substrate material. Its chemical composition is shown in Table 1.

Corresponding author: Jun Li E-mail: jacob_lijun@sina.com

Table 1. Chemical composition of the substrate material wt%

Al	V	Fe	N	C	H	O	Ti
6.5	4.26	0.22	0.03	0.07	0.01	0.14	Bal.

The coating alloy was NiCrBSi alloy powder, and the chemical composition is shown in Table 2.

Table 2. Chemical composition of NiCrBSi alloy wt%

Cr	B	Si	Fe	C	Ni
14.0-18.0	3.0-4.5	3.5-5.5	≤5.0	0.60-1.00	Bal.

Ti6Al4V alloy was machined into the form of cylinders of 50 mm in diameter and 10 mm in length. The substrate surface was degreased in acetone. The organic adhesive (isopropanol) was applied to the surfaces evenly, and then the powders (about 6 g) were preplaced on Ti6Al4V and pressurized with a press force of 58800 N by a hydraulic press instrument to form a layer of 1.0 mm in thickness. The compactness of the obtained coating by the cold press process was higher, which would contribute to suppressing the formation of gas holes. Laser cladding was carried out using an HL-5000 type CO_2 gas laser with an applied power of 2.0 kW, a beam diameter of 5 mm, and a scanning speed of 5 mm/s.

A Rigaku D/mas 2550V X-ray diffractometer (XRD) with Cu K_α radiation was used to analyze the phases of the coating. An S-3400 scanning electron microscope (SEM) coupled with an energy dispersive spectrometer (EDS) was employed to characterize the microstructure. An HV-50Z-type Vickers hardness tester was used to measure the microhardness of different phases with different morphologies, and the load was 490 mN. The microhardness profile of the coating cross-section was also tested with the load of 1.96 N. The cross-section of the sample was prepared by polishing on a Buehler Phoenix 4000 sample preparation system and then rinsed with alcohol and acetone. The sample was eroded by the mixture etchant consisting of 35vol% HNO_3 + 65vol% H_2O + (0.5-1 mL) HF, and the erosion time was about 10 s.

3. Results and discussion

3.1. Thermodynamic predictions

Various chemical reactions may occur in the coating during the process of laser cladding, which result in some new compounds formed. The calculation of thermodynamic data for the cladding system is helpful for predicting which reaction can occur and which phase can be synthesized in the coating. The application of thermodynamics requires the consideration of all possible reactions occurring in the coating. The main components of the used cladding materials are Ti-Ni-B-C-Cr. The reactions between Ti-B, Ti-C, Cr-B, Cr-C, Ni-B, and Ni-Ti are considered.

Ti-B system:

$$Ti + B = TiB \quad (1)$$

$$Ti + 2B = TiB_2 \quad (2)$$

Ti-C system:

$$Ti + C = TiC \quad (3)$$

Cr-B system:

$$B + Cr = CrB \quad (4)$$

$$2B + Cr = CrB_2 \quad (5)$$

Cr-C system:

$$C + 4Cr = Cr_4C \quad (6)$$

$$6C + 23Cr = Cr_{23}C_6 \quad (7)$$

$$3C + 7Cr = Cr_7C_3 \quad (8)$$

$$2C + 3Cr = Cr_3C_2 \quad (9)$$

Ni-B system:

$$3B + 4Ni = Ni_4B_3 \quad (10)$$

$$B + Ni = NiB \quad (11)$$

Ni-Ti system:

$$3Ni + Ti = Ni_3Ti \quad (12)$$

$$Ni + Ti = NiTi \quad (13)$$

$$Ni + 2Ti = NiTi_2 \quad (14)$$

The changes in standard Gibbs free energy of these reactions were calculated by using thermodynamic data [17]. It is evident that $\Delta G^{\ominus}$ of all reactions is negative in the temperature range shown in Fig. 1, indicating that these reactions can spontaneously occur in thermodynamics. At the same temperature, the spontaneous trends of the above chemical reactions are given as follows: (7)>(2)>(8)>(3)>(1)>(12)>(6)>(9)>(13)>(5)>(11)>(14)>(4)>(10). This conclusion demonstrates that TiB_2 and TiC can be formed in

preference to the majority of other compounds, that is, TiB_2 and TiC reinforcements can be in situ synthesized in the coating.

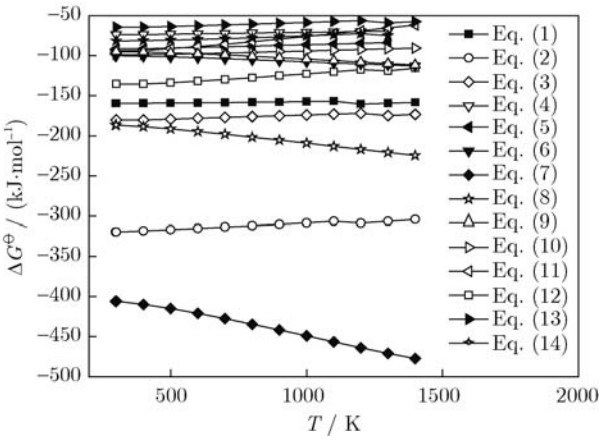

Fig. 1. Changes of the standard Gibbs free energy as a function of temperature for reactions possibly occurred in the cladding materials.

3.2. XRD analysis

Phase constituents of the coating are identified from the XRD pattern shown in Fig. 2. The coating mainly consists of γ, TiB_2, TiC, CrB, and Ni_3B phases. According to the results of XRD analysis, TiB_2 and TiC were in situ synthesized during laser cladding as predicted by thermodynamic analyses. Some diffraction peaks with low intensities were not identified because their diffraction angles are very close to each other or even overlapped. According to the results of thermodynamic analyses, these diffraction peaks most likely coincide with the compounds predicted by thermodynamics.

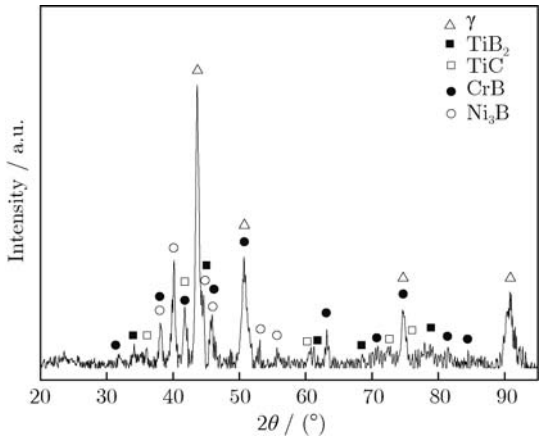

Fig. 2. XRD pattern of the coating.

3.3. Microstructural characterization

Fig. 3 shows the SEM images of the cross section from the coating. The morphology of the whole cross section is shown in Fig. 3(a). The surface of the coating is comparatively smooth, the coating is free from pores and cracks, and the maximum thickness of the coating is about 1.0 mm. The interface between the coating and the substrate is very clear and continuous; no delamination is observed, indicating that it has an excellent metallurgical bond with the substrate. A more detailed SEM image of the interface is shown in Fig. 3(b). Four zones with different morphological characteristics can be observed: the coating, the dilution zone (DZ), the heat-affected zone (HAZ), and the substrate. The thicknesses of DZ and HAZ are about 150 and 100 μm, respectively. Under the radiation of the laser beam, cladding alloy powder and a part of the substrate surface were melted. Due to the interdiffusion of atoms, a DZ including all the atoms of the two parts was formed. The content of alloy elements in the dilution zone is between those in the coating and in the substrate. Alloy elements diffused into the Ti alloy substrate from the coating, which contributes to forming an excellent metallurgical bonding between them. Furthermore, the DZ plays the role of buffer, avoids stress concentration at the interface region, which is caused by the sudden transition between the coating with high hardness and the substrate with low hardness, and then avoids crack initiation.

As seen in Fig. 3(c), the microstructure of the coating is uniform, and plenty of coarse blocky and fine strip-shaped reinforcements are dispersively distributed in the γ matrix. The microstructure shown in the low-powder image actually appears rather simple; however, a closer inspection reveals that it is not the case. As shown in Figs. 3(d) and 3(e), the microstructure of the coating is mainly composed of coarse black blocky phase (C1), fine flower-like or equiaxial phase (C2), fine acicular phase (C3), and the matrix (C4). The black blocky phase with a mean size of about 5-10 μm presents the regular shape (generally quadrilaterals and hexagons), and the interfaces with the matrix possess a faceted feature. The size of flower-like or equiaxial particles is about 1-3 μm. The fine acicular phase with a mean diameter of 1-2 μm and a typical length of 5-10 μm is uniformly distributed in the coating.

EDS spot analysis was used to ascertain the chemical composition of those phases with different morphologies, as shown in Fig. 4 (four red crisscross spots) and Table 3. The results indicate that the black blocky phase is rich in Ti and B. The flower-like or equiaxial phase mainly consists of Ti and C. The strip-shaped phase is mainly composed of Cr, B, and a small quan-

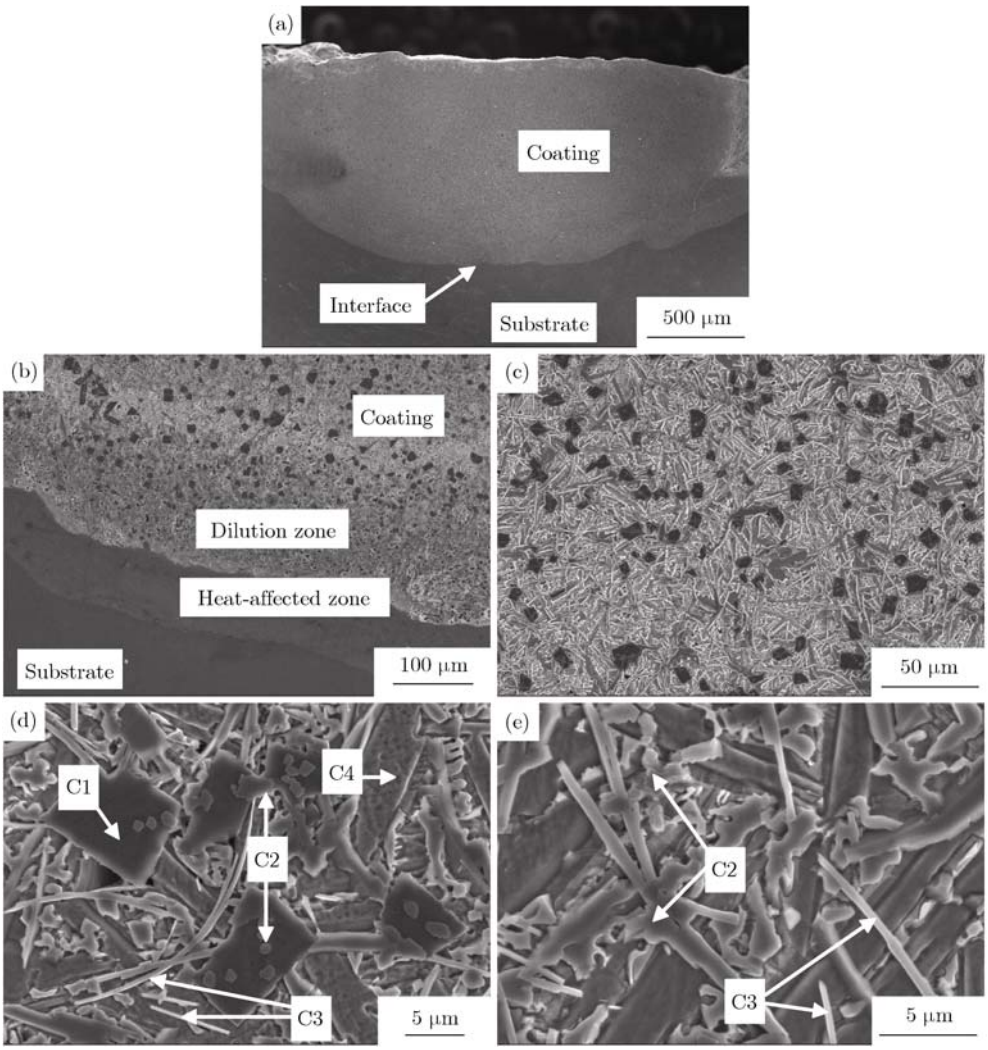

Fig. 3. SEM images of the cross section from the coating: (a) the whole coating; (b) the interface; (c), (d), (e) microstructures of the coating in different magnifications.

tity of C. According to the results of XRD analyses, it can be concluded that black blocky phases (C1), flower-like or equiaxial phases (C2), and fine acicular phases (C3) are TiB_2, TiC, and CrB, respectively. By calculation (as shown in Table 3), the Ti/B atomic ratio is less than 1/2 in black blocky phases, and the Cr/B ratio is less than 1/1 in fine acicular phases. The main reason is that the atomic number of B element is 5, and that is light element. When analyzed quantitatively, the calculated content of light element may be a bit high. The Ti/C ratio in flower-like or equiaxial phases is approximately 1/1. The matrix (C4) is the γ solid solution phase in which Ni is solvent, and the other elements are solutes.

To further confirm the distribution of different elements within the whole microstructure, map scanning was carried out using EDS. The results are depicted in Fig. 5. Fig. 5(a) shows a backscattered electron (BSE) image of the coating, and three phases with different appearances are distributed in the matrix. As shown in Fig. 5(b), Ti element is mainly distributed in the black blocky phase and the flower-like or equiaxial phase, and a small amount of Ti can be observed in the other zone. Ni mainly exists in the matrix, and little Ni is found in three kinds of reinforcements, as can be seen in Fig. 5(c). Figs. 5(d) and 5(e) exhibit that B and C are rich in the black blocky phase and the flower-like or equiaxial phase, respectively. As in conjunction with Fig. 5(b), it is evident that the black blocky phase is composed of Ti and B, and the flower-like or equiaxial phase is rich in Ti and C. Fig. 5(f) reveals that Cr is mainly found in the fine acicular phase. The results of map scanning are consistent with the previous EDS spot analysis.

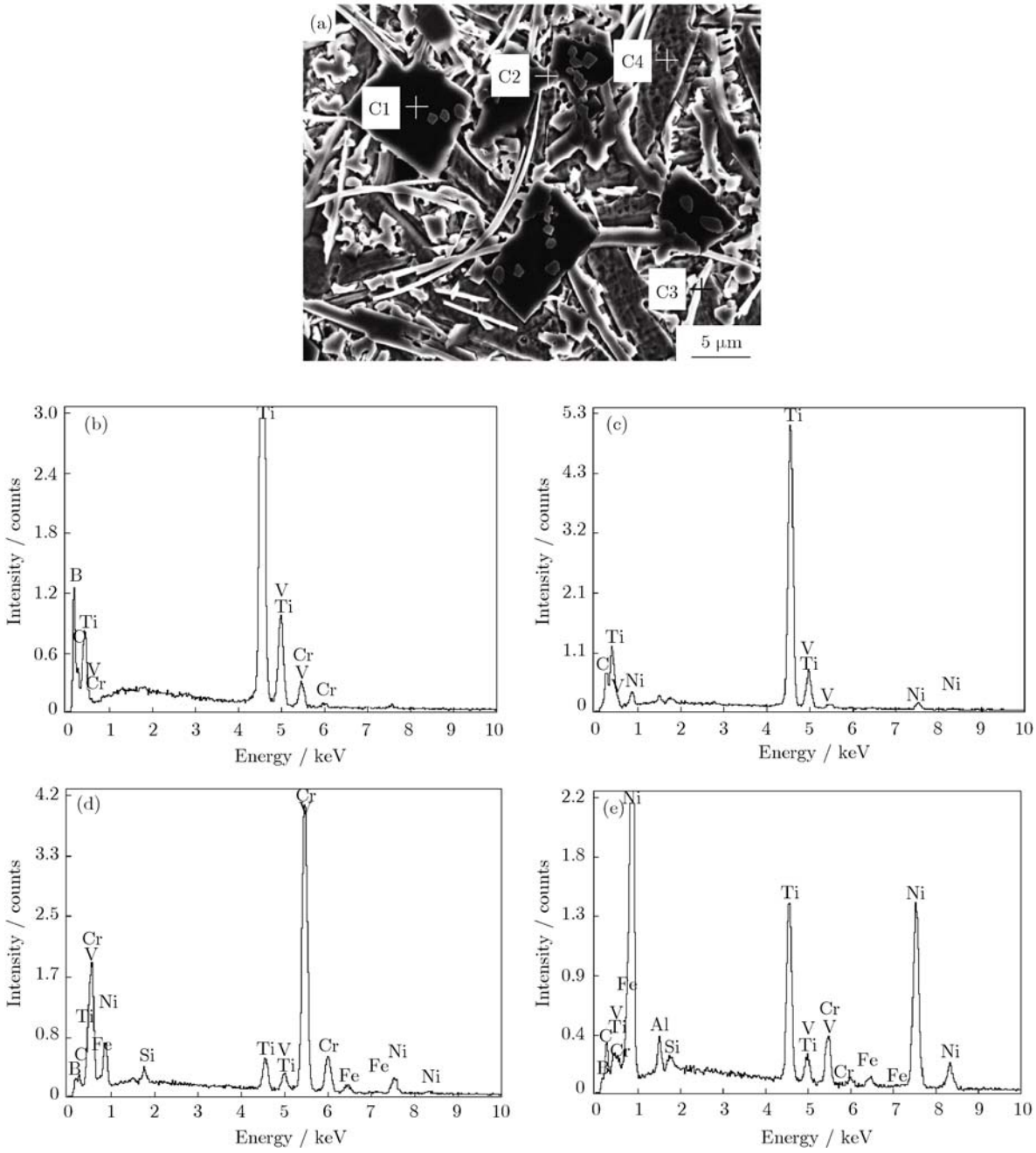

Fig. 4. EDS spot analysis showing the content of phases with different morphologies: (a) SEM image; (b) C1; (c) C2; (d) C3; (e) C4.

Table 3. Chemical composition of phases with different morphologies wt%

Phase	Ti	B	C	Ni	Cr	Al
C1	33.06	55.43	08.28	—	01.92	—
C2	40.87	—	39.11	11.02	04.25	02.33
C3	03.14	30.14	05.85	07.53	48.58	—
C4	11.90	21.40	08.78	49.99	04.81	01.00

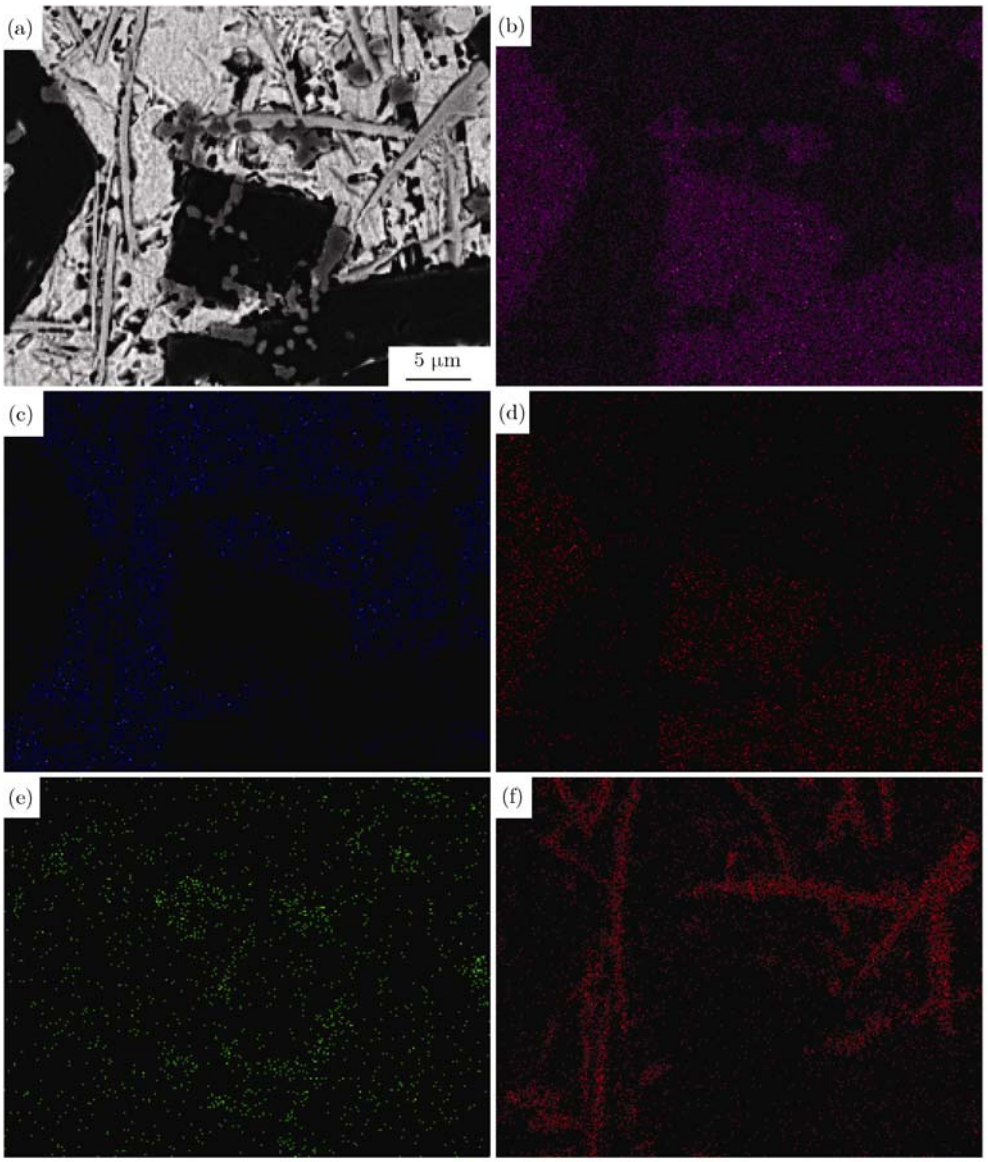

Fig. 5. EDS map scanning results for different elements: (a) BSE image; (b) Ti; (c) Ni; (d) B; (e) C; (f) Cr.

The hardness measurement of phases with different morphologies is important for the evaluation of mechanical properties of the coating. By means of hardness testing, four phases mentioned above were analyzed. Hardness indentations of phases with different morphologies are circled by white rings as shown in Fig. 6. Table 4 lists the Vickers hardness of the phases. The theoretical hardness values of TiB_2 and TiC are about $Hv_{0.05}$ 3400 and $Hv_{0.05}$ 3000, respectively, which are generally higher than the experimental results; this may be attributed to the measurement error. The test load is low, so the indentation depth and the area of indentation are not obvious (as shown in Fig. 6), which cause the measurement error. The hardness of TiB_2, TiC, and CrB is much higher than that of the matrix. The dispersive distribution of such high hardness reinforcements could cause the increase in hardness of the whole coating.

3.4. Microhardness profile

The microhardness profile along the depth direction of the coating is shown in Fig. 7. There are three regions on the microhardness curve, corresponding to the cladding zone, HAZ, and the substrate. The thickness of the coating is about 1.0 mm. The HAZ is narrow with just one point on the microhardness curve, and the thickness is about 100 μm, which has been confirmed on the SEM image shown in Fig. 3(b). The DZ cannot be identified clearly from the microhardness profile. As shown in Fig. 3(b), the morphology of DZ is very similar to that of the coating except the tiny difference in the volume fraction of TiB_2 particles, so the

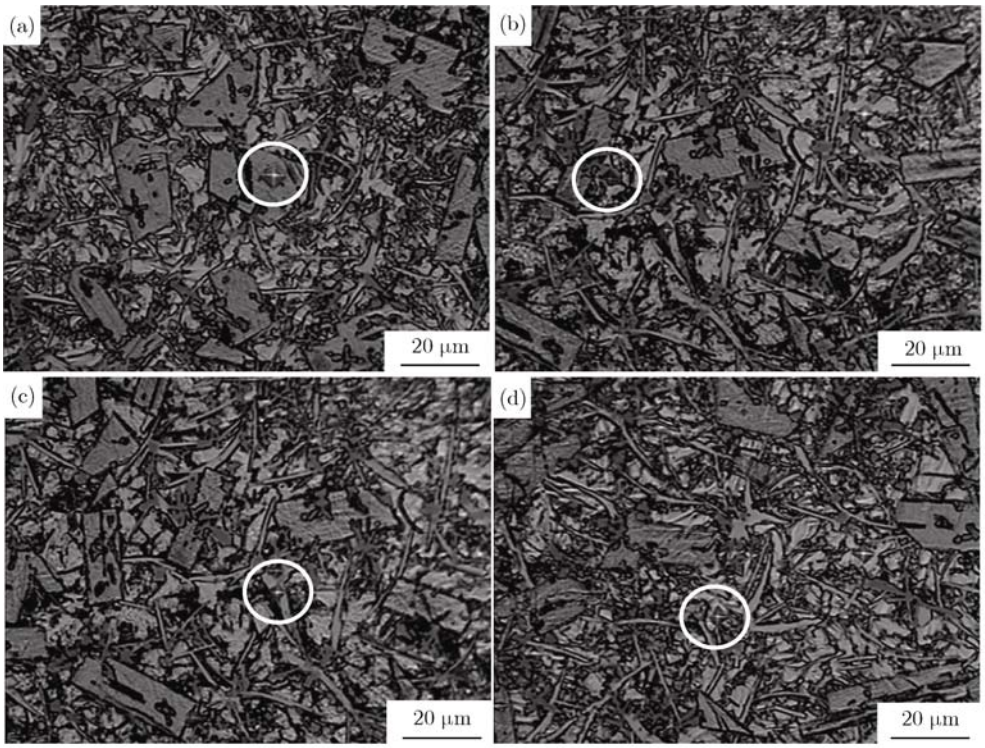

Fig. 6. Hardness indentations of phases with different morphologies in the coating: (a) C1; (b) C2; (c) C3; (d) C4.

Table 4. Vickers hardness ($Hv_{0.05}$) of phases with different morphologies in the coating

Black blocky phase (C1)	2208.7
Flower-like or equiaxial phase (C2)	1981.0
Strip-shaped phases (C3)	1362.3
Matrix (C4)	846.9

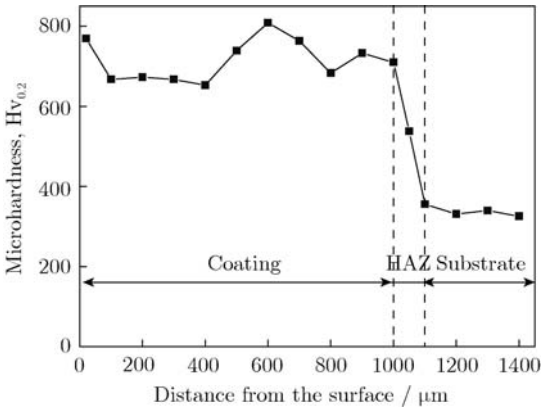

Fig. 7. Microhardness profile along the depth direction of the coating.

fluctuation in microhardness from the coating to DZ is not obvious. The average of the microhardness was approximately $Hv_{0.2}$ 700 in the coating, $Hv_{0.2}$ 550 in the HAZ, and $Hv_{0.2}$ 320 in the substrate. The hardness of the coating is obvious higher than that of the substrate due to the dispersion strengthening of reinforcements. The hardness distribution through the coating has a big fluctuation with the change in distance from the surface, which should mainly be attributed to the size of TiB_2 particles. Compared with the other reinforcements, such as TiC and CrB, TiB_2 particles are very coarse (about 10 μm) and distribute in a scattered manner in the coating. During the microhardness test, when a load is applied to the zone in which the volume fraction of TiB_2 particles is very small, the obtained hardness value is low. On the contrary, the high hardness value can be obtained in the zone composed of a large number of TiB_2 particles. The refining and uniform dispersion of TiB_2 particles in the coating will contribute to the decrease of hardness fluctuation.

4. Conclusions

(1) A Ni-based composite coating reinforced by in situ synthesized TiB_2 and TiC particles was fabricated on Ti6Al4V by laser cladding. The coating mainly consists of a large number of reinforcements (black massive particle shaped TiB_2, fine flower-like or equiaxial TiC, and acicular CrB) and the matrix (γ solid solution phase in which Ni is solvent and the other elements are solutes).

(2) The hardness of TiB_2 and TiC reinforcement

phases is much higher than that of the other phases. It is for this reason that the dispersive distribution of such high hardness reinforcements results in the increase in hardness of the whole coating.

(3) The average of the microhardness was approximately $Hv_{0.2}$ 700 in the coating, $Hv_{0.2}$ 550 in the HAZ, and $Hv_{0.2}$ 320 in the substrate. The hardness of the coating is obviously higher than that of the substrate due to the dispersion strengthening of reinforcements.

Acknowledgements

This work was financially supported by the National Natural Science Foundation of China (No. 51002093), Shanghai Science and Technology Development Foundation (No. 08QA14035) and Shanghai Leading Academic Discipline Project (No. J51402).

References

[1] X.B. Liu and R.L. Yu, Effects of La_2O_3 on microstructure and wear properties of laser clad γ/Cr_7C_3/TiC composite coatings on TiAl intermatallic alloy, *Mater. Chem. Phys.*, 101(2007), p. 448.

[2] J.J. Candel, V. Amigó, J.A. Ramos, and D. Busquets, Sliding wear resistance of TiC reinforced titanium composite coating produced by laser cladding, *Surf. Coat. Technol.*, 204(2010), p. 3161.

[3] D.S. Wang, Z.J. Tian, L.D. Shen, Z.D. Liu, and Y.H. Huang, Research states of laser surface modification technology on titanium alloys, *Laser Optoelectron. Prog.*, 45(2008), p. 24.

[4] J.D. Majumdar and L. Li, Development of titanium boride (TiB) dispersed titanium (Ti) matrix composite by direct laser cladding, *Mater. Lett.*, 64(2010), p. 1010.

[5] Y.L. Yang, D. Zhang, W. Yan, and Y.R. Zheng, Microstructure and wear properties of TiCN/Ti coatings on titanium alloy by laser cladding, *Opt. Laser Eng.*, 48(2010), p. 119.

[6] J. Nurminen, J. Näkki, and P. Vuoristo, Microstructure and properties of hard and wear resistant MMC coatings deposited by laser cladding, *Int. J. Refract. Met. Hard Mater.*, 27(2009), p. 472.

[7] J. Li, Z,S. Yu, H.P. Wang, and M.P. Li, Microstructural evolution of titanium matrix composite coatings reinforced by in situ synthesized TiB and TiC by laser cladding, *Int. J. Miner. Metall. Mater.*, 17(2010), p. 481.

[8] Y.P. Pu, B.G. Guo, J.S. Zhou, S.T. Zhang, H.D. Zhou, and J.M. Chen, Microstructure and tribological properties of in situ synthesized TiC, TiN, and SiC reinforced Ti_3Al intermetallic matrix composite coatings on pure Ti by laser cladding, *Appl. Surf. Sci.*, 255(2008), p. 2697.

[9] B.G. Guo, J.S. Zhou, S.T. Zhang, H.D. Zhou, Y.P. Pu, and J.M. Chen, Phase composition and tribological properties of Ti-Al coatings produced on pure Ti by laser cladding, *Appl. Surf. Sci.*, 253(2007), p. 9301.

[10] R. Banerjee, A. Genç, D. Hill, P.C. Collins, and H.L. Fraser, Nanoscale TiB precipitates in laser deposited Ti-matrix composites, *Scripta Mater.*, 53(2005), p. 1433.

[11] Y. Wang and H.M. Wang, Wear resistance of laser clad Ti_5Ni_3Si reinforced intermetallic composite coatings on titanium alloy, *Appl. Surf. Sci.*, 229(2004), p. 81.

[12] J. Li, W.G. Li, and H.Y. Zhang, Ni-based composite coatings reinforced by TiB/WC synthesized in situ on stainless steel by laser cladding, *Mater. Mech. Eng.*, 32(2008), p. 34.

[13] X.H. Wang, M. Zhang, Z.D. Zou and S.Y. Qu, Microstructure and properties of laser clad TiC + NiCrBSi + rare earth composite coatings, *Surf. Coat. Technol.*, 161(2002), p. 195.

[14] R.L. Sun, J.F. Mao, and D.Z. Yang, Microstructural characterization of NiCr1BSiC laser clad layer on titanium alloy substrate, *Surf. Coat. Technol.*, 150(2002), p. 199.

[15] R.L. Sun, Y. Tang, and X.J. Yang, Microstructure and tribological properties of In-situ synthesized TiB_2-TiC/Ni based composite coating by laser cladding, *Trans. Mater. Heat Treat.*, 25(2004), p. 1000.

[16] L.F. Cai, Y.Z. Zhang, and L.K. Shi, Microstructure and formation mechanism of titanium matrix composites coating on Ti-6Al-4V by laser cladding, *Rare Met.*, 26(2007), p. 342.

[17] D.L. Ye and J.H. Hu, *Practical Inorganic Thermodynamics Manual*, Metallurgical Industry Press, Beijing, 2002, p. 57.